M. Sc. Thesis
on

MESA Stellar modelling for determining the age of stars using Asteroseismology

submitted by

Vishal Sai Vetrivel

Roll No: P0211557

Under the guidance of

Prof. Shravan Hanasoge, TIFR

Department of Physical Sciences

Centre for Excellence in Basic Sciences

Mumbai - 400098

Submitted on November 2025

Declaration

I, Vishal Sai Vetrivel (Roll No. P0211557), hereby declare that this thesis titled "MESA Stellar modelling for determining the age of stars using Asteroseismology" submitted to Centre for Excellence in Basic Sciences towards the partial requirement of my Integrated M. Sc. in Physics, is a culmination of my original research effort. All contributions from others to this thesis are cited and acknowledged explicitly.

This work was done under the guidance of Prof. Shravan Hanasoge at Tata Institute of Fundamental Research.

Acknowledgements

I would like to thank my guide Prof. Shravan Hanasoge for providing me the opportunity to work with his group. I would also like to thank Dr. Meenakshi Gaira, whose collaboration was essential for this project.

I would also like to thank Prof. H M Antia who gave invaluable advice on MESA, convective models and writing this report among many other things.

I would also like to thank Dr. Warrick Ball, Dr. Ebraheem Farag and other members of the MESA user list for being extremely helpful in the implementation of the CM model into MESA.

I am also extremely grateful to the ADS for publishing such a large wealth of knowledge for free without which this project would have been impossible. The same goes for Prof. Jørgen Christensen-Dalsgaard whose publicly uploaded Lecture notes, on stellar oscillations, built the foundation which made this project possible.

I would also like to thank my family who took the time to proofread this report and have supported me wholeheartedly in my pursuit of science.

I am also thankful to my room-mate and good friend Dhiyanesh whose ability to find stray brackets and typos is better than most editors.

Certificate

This is to certify that Vishal Sai Vetrivel, student of UM DAE CEBS, has undertaken project work from May 2025 to December 2025 under the guidance of Prof. Shravan Hanasoge, TIFR.

This submitted report titled MESA Stellar modeling for determining the age of stars using Asteroseismology is towards the academic requirements of the Integrated M. Sc. course at UM DAE CEBS.

27/11/25

Signature of Student
Vishal Sai Vetrivel
UM DAE CEBS

Signature of Guide
Prof. Shravan Hanasoge
TIFR

Department of Physical Sciences
Centre for Excellence in Basic Sciences
Mumbai - 400098

Abstract

The determination of stellar age for far away stars is a challenge due to the amount of data available to us. The conventional method for determining stellar age does not make full use of this limited data due to the lack of understanding behind mixed modes and g modes. This thesis seeks to make full use of all the seismological data available to us by using modern theory and computational resources such as MESA. We also take into consideration methods, such as surface correction, to account for effects that are yet to be well understood. It is expected that this will lead to a significant increase in reliable stellar age measurements.

Contents

1. Introduction

Asteroseismology is the study of oscillations in stars. The path of sound inside a star depends on the local speed of sound, which in turn depends on the local temperature and chemical composition. These oscillations are sensitive to different parts of the star which allow the study of the structure of the star which would normally be impossible to infer from overall properties such as brightness or surface temperature.

Asteroseismology shares a close relationship with Helioseismology as the underlying physics is the exact same. The difference between the fields arises from the difference in data available to study. In the case of the Sun, we are relatively closer as observers and as a result are able to record oscillations over the surface in the form of Doppler velocities. This spatial resolution allows us to extract more information from the oscillations themselves. In the case of faraway stars, we only have access to surface integrated variables such as luminosity. This severely limits the information that can be extracted.

To put the difference into numbers, in the Sun even with ground based observatories such as GONG we can easily get frequencies with degree up to 150. With space based observatories such as HMI or MDI this can go up to degrees of 300. This is in stark contrast to the other faraway stars where we hardly get frequencies of degrees up to 3. This lack of information makes it difficult to perform techniques such as solving inverse problems for rotation which are relatively easier in the Sun.

Without seismology the only information available are luminosity, T_{eff}, metallicity, etc. This is not enough to sufficiently constrain stellar models. The measured frequencies also provide us additional input such as $\Delta\nu$ and period spacing which can be used to further constrain stellar models. This allows us to determine mass and age of stars. Age is a difficult value to determine for field stars (stars outside a globular cluster). However, the ages of Red Giants are generally well constrained by their mass but uncertainty in their mass can lead to large variance in the age.

1.1 Data used in this Study

The data for this thesis were taken from the Kepler space telescope (Borucki et al., 2010). The Kepler Space Telescope was launched by NASA in 2009. It has since been retired in 2018, due to the fuel for its reaction control system running out. It was succeeded by the Transiting Exoplanet Survey Satellite or TESS, launched in 2018. Kepler followed an Earth trailing heliocentric orbit. It houses a single differential photometer that with a wide field of view (115 square degrees) that continuously and simultaneously observes the brightness of nearly 150,000 stars. The cadence of these observations are either 1 minute or 30 minutes. The 1 minute cadence data is only downloadable for 512 stars at a time. This is due to the limit on data downloadable from the satellite. This is a problem for asteroseismological study of main sequence stars but is not a major issue for Red Giants as their periods are higher and can be studied well even by the larger cadence data. This allows asteroseismological studies on nearly 16,000 Red Giants from Kepler's Data.

Kepler had two phases of observation. The first phase lasted about 4 years which included measurements of many stars with a suitable duration to perform seismological studies. However, following the failure of two reaction wheels it became impossible to keep the satellite pointed at the same field for long periods. This phase was called K2 and it was still possible to obtain light curves of durations lesser than 5 months but this is not always enough for seismological studies. The data in this study are mostly from the first phase of the satellite's operation.

The data usually consists of a light curve with a duration of 3 to 4 years. This data were downloaded and stored in various repositories. They can be downloaded conveniently using the `lightkurve` python library. This allows us to easily download the time series data from the Kepler mission and perform simple processing to it. As part of the data collection, `lightkurve` is used to download all the data on a particular star, stitch them together, remove outliers and generate a periodogram. This is then used to extract a power spectrum for frequencies.

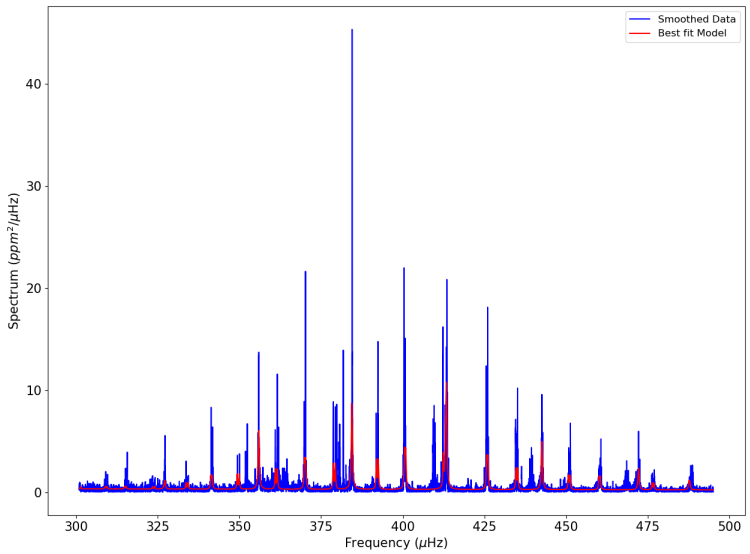

Figure 1.1: An example power spectrum for the star KIC 7341231.
The fitting is done by MCMC fitting. This is an extremely time consuming process and takes many hours if not days.

2. Theory of Stellar Oscillations

A brief overview on the theory of stellar oscillations is included here. Most of the derivations given in this section can be found in Prof. Jørgen Christensen Dalsgaard's Lecture Notes (Christensen-Dalsgaard).

In the perturbative treatment of stellar oscillations, the hydrodynamical equations are solved under the assumption that there is a hydrostatic spherically symmetric equilibrium about which oscillations are perturbations. This is true for many stars but not for all of them. Notably Cepheids exhibit large amplitude oscillations that cannot be studied as perturbations to an equilibrium state.

In this derivation we must deal with two different descriptions of quantities. The **Eulerian** description gives us the value of a quantity at a specific position and time i.e. $p(\boldsymbol{r}, t)$. Whereas the **Lagrangian** description follows an element of the gas. We label functions of any properties in the Lagrangian description using time and the initial position $\boldsymbol{r_0}$ which is the position of the fluid element at some time t_0 i.e. $p(\boldsymbol{r_0}, t)$.[1]

The time derivative when following the motion of the fluid element is given by

$$\frac{d\psi}{dt} = \left(\frac{\partial \psi}{\partial t}\right)_{\boldsymbol{r}} + \left(\frac{\partial \boldsymbol{r}}{\partial t} \cdot \nabla\right) \psi = \left(\frac{\partial \psi}{\partial t}\right)_{\boldsymbol{r}} + (\boldsymbol{v} \cdot \nabla)\, \psi, \tag{2.1}$$

here ψ is any quantity such as density or pressure, $\boldsymbol{v}$ is the velocity of the fluid element. The time derivative d/dt following the motion is called the material time derivative and $\partial/\partial t$ is known as the local time derivative.

Some other basic equations used are the equation of continuity

$$\frac{\partial \rho}{\partial t} + \operatorname{div}(\rho \boldsymbol{v}) = 0, \tag{2.2}$$

here ρ is the density and $\boldsymbol{v}$ is the velocity of the fluid element.

[1] All bold face variables are vectors.

Under stellar conditions we can usually ignore viscosity. This gives us the equation of motion as

$$\rho\frac{\partial \boldsymbol{v}}{\partial t}+\rho\boldsymbol{v}\cdot\nabla\boldsymbol{v}=-\nabla p-\rho\nabla\Phi, \tag{2.3}$$

where p is pressure of the fluid element and Φ is gravitational potential and it satisfies Poisson's equation

$$\nabla^2\Phi=4\pi G\rho, \tag{2.4}$$

or the integral form

$$\Phi\left(\boldsymbol{r},t\right)=-G\int_V\frac{\rho\left(\boldsymbol{r}',t\right)\mathrm{d}V}{|\boldsymbol{r}-\boldsymbol{r}'|}, \tag{2.5}$$

here G is the gravitational constant. In stars, if the time scale for heat exchange is larger than the oscillation time period then the adiabatic assumption can be made. This is often the case for oscillations inside the star, but need not be true near the surface where the sound speed is low. This is generally not an issue as the surface effects can be isolated and compensated for in other ways (see Chapter 5). This allows us to use the relation

$$\frac{dp}{dt}=\frac{\Gamma_1 p}{\rho}\frac{d\rho}{dt}, \tag{2.6}$$

here Γ_1 is an adiabatic exponent defined by $\Gamma_1=\left(\frac{\partial\ln p}{\partial\ln\rho}\right)_{ad}$. To study these stellar oscillations we shall assume small perturbations about a spherically equilibrium state defined by

$$\nabla p_0=\rho_0\boldsymbol{g}_0. \tag{2.7}$$

We can assume this as most oscillations are small compared to the length scales of the star. This is not always the case for example in Cepheid variables. However, since they aren't studied in this report we may use this assumption. We also assume a spherically symmetric equilibrium state as doing so allows us to separate the radial and angular dependencies allowing us to form a system of ordinary differential equations. The perturbations to this state are given by

$$p(\boldsymbol{r},t)=p_0(\boldsymbol{r},t)+p'(\boldsymbol{r},t), \tag{2.8}$$

where p' is the Eulerian perturbation. The Lagrangian perturbation would be

$$\delta p=p'(\boldsymbol{r}_0)+\boldsymbol{\delta r}\cdot\nabla p_0. \tag{2.9}$$

If we account for non-radial oscillations we can assume scalar perturbations to have the form

$$p'\left(r,\theta,\phi,t\right)=\sqrt{4\pi}\tilde{p}'\left(r\right)Y_l^m\left(\theta,\phi\right)\exp\left(-i\omega t\right), \tag{2.10}$$

where $Y_l^m(\theta,\phi)$ are spherical harmonics with degree l and azimuthal order m, ω is the frequency. For vector quantities such as displacement ($\boldsymbol{\delta r}$) the form can be taken as

$$\boldsymbol{\delta r}=\sqrt{4\pi}Re\left\{\left[\tilde{\xi}_r\left(r\right)Y_l^m\left(\theta,\phi\right)\boldsymbol{a}_r+\tilde{\xi}_h\left(r\right)\left(\frac{\partial Y_l^m}{\partial\theta}\boldsymbol{a}_\theta+\frac{1}{\sin\theta}\frac{\partial Y_l^m}{\partial\phi}\boldsymbol{a}_\phi\right)\right]\exp\left(-i\omega t\right)\right\}. \tag{2.11}$$

When perturbations of these forms are applied to the basic equations, with some manipulation, give the following three equations that constitute a fourth order system of complete set of differential equations.

$$\frac{d\xi_r}{dr}=-\left(\frac{2}{r}+\frac{1}{\Gamma_1 p}\frac{dp}{dr}\right)\xi_r+\frac{1}{\rho c^2}\left(\frac{S_l^2}{\omega^2}-1\right)p'+\frac{l\left(l+1\right)}{\omega^2 r^2}\Phi', \tag{2.12}$$

$$\frac{dp'}{dr}=\rho\left(\omega^2-N^2\right)\xi_r+\frac{1}{\Gamma_1 p}\frac{dp}{dr}p'-\rho\frac{d\Phi'}{dr}, \tag{2.13}$$

$$\frac{1}{r^2}\frac{d}{dr}\left(r^2\frac{d\Phi'}{dr}\right)=4\pi G\left(\frac{p'}{c^2}+\frac{\rho\xi_r}{g}N^2\right)+\frac{l\left(l+1\right)}{r^2}\Phi', \tag{2.14}$$

here S_l is the characteristic acoustic frequency and is given by

$$S_l^2=\frac{l\left(l+1\right)c^2}{r^2}=k_h^2c^2, \tag{2.15}$$

where c^2 is squared sound speed and k_h is horizontal wavenumber. N^2 is the Brunt–Väisälä frequency given by

$$N^2 = g_0 \left(\frac{1}{\Gamma_{1,0}} \frac{d \ln p_0}{dr} - \frac{d \ln \rho_0}{dr} \right). \tag{2.16}$$

To supplement these equations we need four boundary conditions. We can determine these conditions by looking at the behaviour at the center and the surface of the star.

$r \to 0$	$r = R$
$\xi_r \sim r^{l-1}$	$\frac{d\Phi'}{dr} + \frac{l+1}{r}\Phi' = 0$
$p', \Phi' \sim r^l$	$\delta p = 0$

We set the $r \to 0$ conditions to ensure that we get regular solutions from the singlular point $r = 0$. The surface condition of $\delta p = 0$ is Lagrangian instead of Eulerian as the due to the perturbations the surface of the star will not be perfectly spherical. The Lagrangian follows the perturbations and hence is the correct description to use for this condition.

We now make the Cowling approximation, which states that we can neglect Φ' when l is large, as the oscillations are trapped near the surface where the density is too low for them to contribute to Φ' and when radial order n is large, as the integrals are over rapidly varying functions and may cancel. This approximation is only used to identify the modes and when actual numerical calculations are done the full expression is used instead. Under this approximation the above equations can be written as

$$\frac{d\xi_r}{dr} = -\left(\frac{2}{r} - \frac{1}{\Gamma_1} H_p^{-1} \right) \xi_r + \frac{1}{\rho c^2} \left(\frac{S_l^2}{\omega^2} - 1 \right) p', \tag{2.17}$$

$$\frac{dp'}{dr} = \rho \left(\omega^2 - N^2 \right) \xi_r - \frac{1}{\Gamma_1} H_p^{-1} p', \tag{2.18}$$

where H_p is the pressure scale height defined as

$$H_p^{-1} = -\frac{d \ln p}{dr}. \tag{2.19}$$

We now neglect the quantities with respect to their derivatives. This is done under the assumption that the eigenfunctions vary on a scale much smaller than r or pressure scale height. This means that $\frac{d\xi_r}{dr} \approx k_r \xi$ but $k_r \gg 1/r$ or $1/H_p$. This is consistent with WKB approximation. This means that the quantities, with some care, can be neglected. This is simplifies things greatly for analysis. Combining the two resulting equations gives

$$\frac{d^2\xi_r}{dr^2} = \frac{\omega^2}{c^2} \left(1 - \frac{N^2}{\omega^2} \right) \left(\frac{S_l^2}{\omega^2} - 1 \right) \xi_r, \tag{2.20}$$

which we will write as

$$\frac{d^2\xi_r}{dr^2} = -K(r)\, \xi_r, \tag{2.21}$$

where

$$K(r) = \frac{\omega^2}{c^2} \left(\frac{N^2}{\omega^2} - 1 \right) \left(\frac{S_l^2}{\omega^2} - 1 \right). \tag{2.22}$$

This equation allows us to study the local behaviour of ξ_r. If $K(r)$ is positive then ξ_r will be oscillatory and if $K(r)$ is negative it will be exponential. This only affects the spatial part of the solution. For the temporal part since the equations only have ω in its squared form we expect the solution to be such that ω^2 is real. This means ω is either purely real or purely imaginary. The former case is an undamped oscillator and the latter case is either exponentially growing or decaying system. Physically this stems from the adiabatic condition which states that the only energy fed into the motion of the system comes from the gravitational field which allows only a dynamical instability.

According to this description the solution oscillates when

$$\text{o1)} \qquad \omega^2 > N^2 \qquad \text{and} \qquad \omega^2 > S_l^2, \tag{2.23}$$

or

$$\text{o2)} \qquad \omega^2 < N^2 \qquad \text{and} \qquad \omega^2 < S_l^2, \tag{2.24}$$

and it is exponential when

$$\text{e1)} \qquad N^2 < \omega^2 < S_l^2, \tag{2.25}$$

or

$$\text{e2)} \qquad S_l < \omega^2 < N^2. \tag{2.26}$$

For any given mode the displacement will be oscillatory in some regions that satisfy o1) and o2) and exponential in the regions in between. In general one of these oscillatory regions will be dominant and the displacement will exponentially fall off away from that region. We refer to this phenomenon as trapping of modes. The places where $K = 0$ and $\omega^2 = N^2$, are called turning points. This is due to the fact that in the interpretation of these waves as acoustic waves, they experience total internal reflection at these points. The frequency of these oscillations are greatly determined by the structure of these dominant regions of oscillation. Since modes are oscillatory in different regions we get a rich sample of data as each mode is sensitive to a different region of the star.

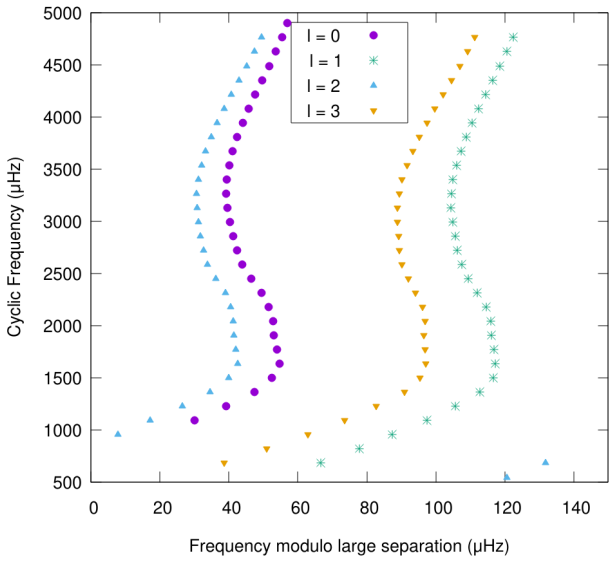

Figure 2.1: An Echelle diagram plotted for the $l = 0, 1, 2, 3$ Solar frequencies.

Modes satisfying o1) are labelled p modes and those satisfying o2) are labelled g modes. Modes that satisfy both the conditions in different parts of the star are termed mixed modes. p modes are also called acoustic modes. They are interpreted as acoustic waves where the dominant restoring force is the pressure gradient. They usually have large frequencies as the condition o1) requires them to be above both $|N|$ and S_l, and S_l is generally larger than $|N|$. p modes are trapped between an inner turning point r_t given by

$$r_t = \frac{\sqrt{l(l+1)}}{\omega} c(r_t), \tag{2.27}$$

and the surface, where c is the sound speed at r_t, ω is the mode frequency and l is the degree of the mode. We can see that high frequency modes penetrate further into the star allowing more analysis on the core. p mode frequencies with $l \ll n$ also have good frequency separation where two consecutive modes with the same degree are spaced in equal intervals. This separation can be obtained from an asymptotic analysis and gives the expression

$$\nu_{nl} \simeq \left(n + \frac{l}{2} + \frac{1}{4} + \alpha\right) \Delta\nu - \left(AL^2 - \delta\right) \frac{\Delta\nu^2}{\nu_{nl}}, \tag{2.28}$$

where

$$A = \frac{1}{4\pi^2 \Delta\nu}\left[\frac{c\,(R)}{R} - \int_0^R \frac{dc}{dr}\frac{\mathrm{d}r}{r}\right], \qquad L = l(l+1). \tag{2.29}$$

This implies the existence of a large frequency separation between two modes of consecutive n values and a small frequency separation between consecutive modes with the same $n + l/2$ for example $n = 2, l = 0$ and $n = 1, l = 2$. This can be seen in Figure (2.1) where $l = 0$ and $l = 2$ modes are closer together and the same is seen for $l = 1$ and $l = 3$.

This can be seen if an Echelle diagram is plotted for the frequencies. An Echelle diagram takes the frequencies and divides them into intervals of large frequency separation and stacks them on top of each other. If the difference between consecutive frequencies is similar then we will see vertical lines. We can see in Figure 2.1 that the Solar frequencies have a good trend in an Echelle diagram.

g modes are trapped gravity waves. Their turning points are determined by where $N = \omega$ is satisfied. A similar pattern to p modes can be found in the periods of g modes. Consecutive radial orders with the same degree l and azimuthal order m are well spaced in intervals called period spacing $\Delta\Pi$.

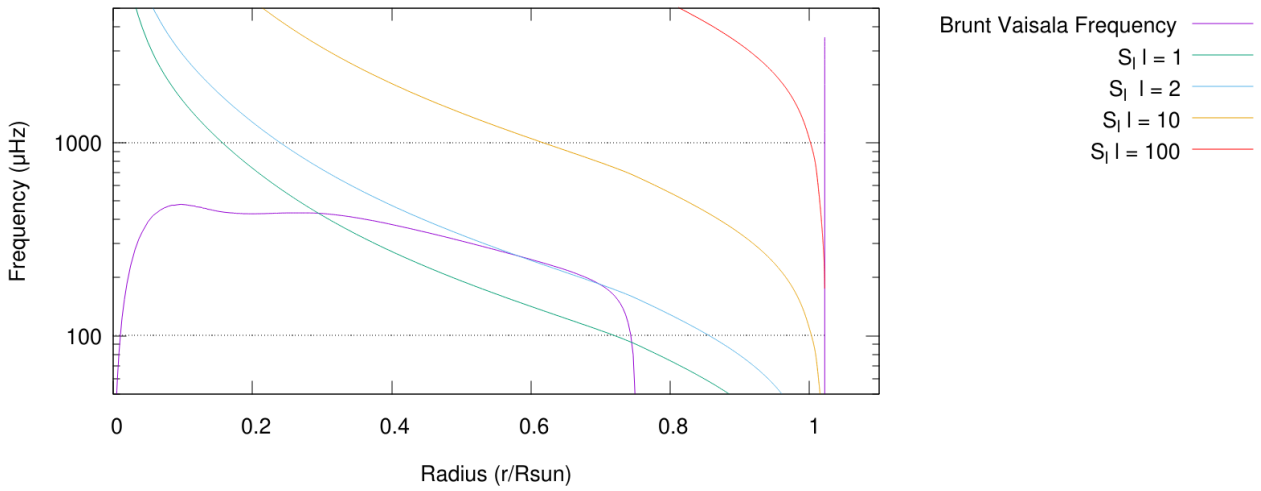

Figure 2.2: Here the solid lines indicate the Brunt-Väisälä Frequency and the Acoustic cut-off frequencies for $l = 1, 2, 10, 100$. The dotted lines represent the typical p and g mode frequencies.

Figure (2.2) shows various frequencies plotted throughout the Sun. It can be seen that as the degree increases the S_l^2 associated with it becomes increasingly trapped near the surface. This leads to all p modes with high degree to be trapped extremely close to the surface. The two dotted lines represent typical p and g mode frequencies with the lower one being g modes and the higher one being p modes. We can see that all g modes are actually mixed modes as near the surface they behave as p modes. Also the large peak in Brunt Väisälä frequency near the surface ensures that all modes are trapped inside the star, since while S_l drops near the surface, N goes up and all the frequencies end up between the two and become evanescent. It is noted that most observed frequencies in the Sun are above 1000 μHz, this means all these frequencies only exhibit p mode behaviour as they are evanescent till the inner turning point of p modes. All the modes that could have g mode behaviour have very low frequencies which are not observed in the Sun.

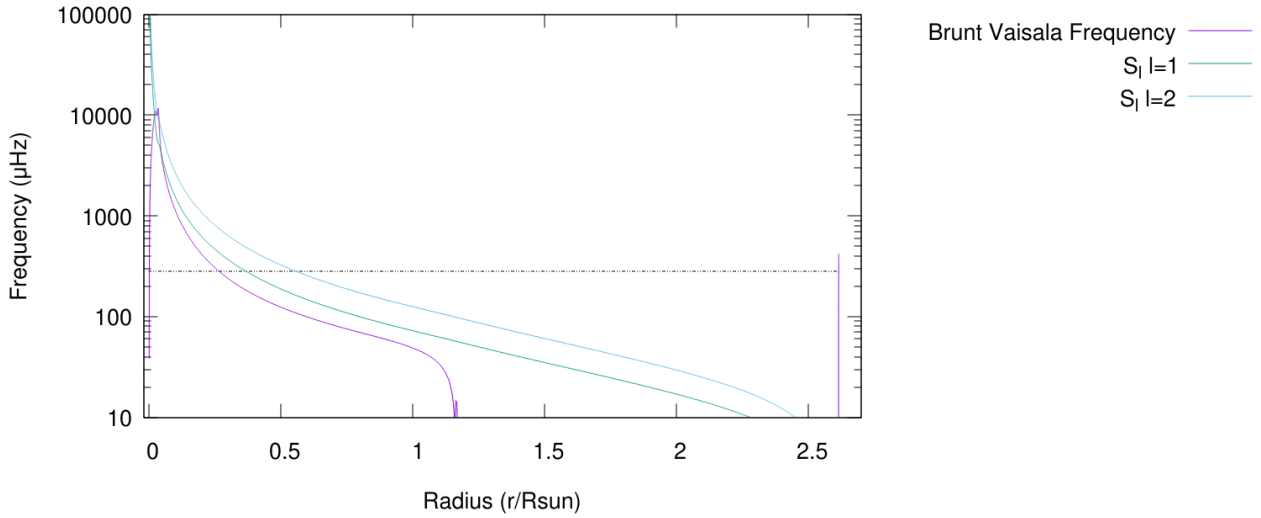

Figure 2.3: Here the solid lines indicate the Brunt-Väisälä Frequency and the Acoustic cutoff frequencies for $l = 1, 2$. The dotted line represents a typical frequency that is observed. It can be seen that at this frequency, the mode is usually mixed and exhibits both p and g mode behaviour.

This is, however, not the case when it comes to Red giants. As seen in Figure 2.3 the $|N|$ is much larger. More importantly, the evanescent region between the g mode region and the p mode region is not large. Combined with the fact that the g mode region is much larger in red giants the $l = 1$ modes end up as mixed modes. These modes exhibit behaviour of both p and g modes to varying extents. This can be readily seen in an Echelle diagram.

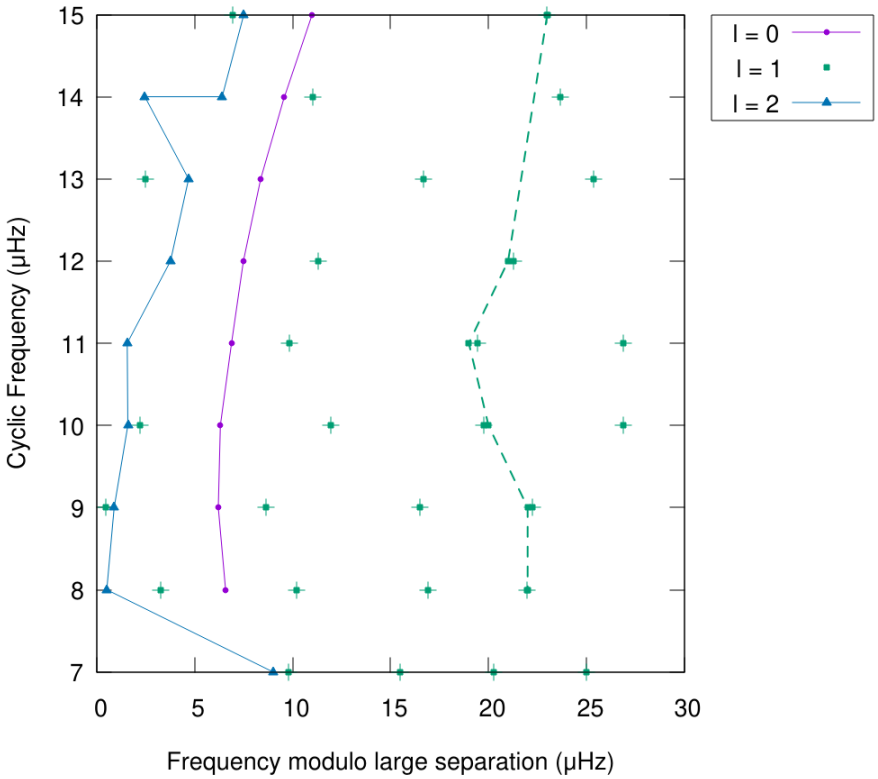

Figure 2.4: Echelle diagram for a computed model for the star KIC 7341231. The $l = 0$ and $l = 2$ show a good pattern whereas the $l = 1$ mixed modes do not seem to have a single frequency separation. The dashed line connects the p dominated modes in $l = 1$ and we see that a rough pattern can be found.

It can be seen that only the $l = 0$ and $l = 2$ modes have consistent frequency separations. The $l = 1$ are mixed modes and therefore do not have a single large frequency separation.

3. MESA Modelling

3.1 Introduction

MESA or Modules for Experiments in Stellar Astrophysics (Paxton et al., 2011) is an open source software suite designed to run experiments in one dimensional stellar evolution. Its modular nature allows users to add any features that are not present through user written hooks and scripts.

MESA is a fully featured stellar structure and evolution library that uses various physics and numerical modules. It provides a clean-sheet implementation of Henyey et al. (1959) with automatic mesh refinement, analytic Jacobians, and coupled solution of structure and compositional equations.

MESA first reads the input files and initializes the physics modules to create a nuclear reaction network and access the EOS and opacity data. MESA receives its basic input from two Fortran namelist files. The first file specifies the type of evolutionary calculation to be performed, the type of input model to use, the source of EOS and opacity data, the chemical composition and nuclear network, and other properties of the input model. The second file specifies the controls and options to be applied during the evolution. After loading the specified starting model into memory the evolution loop is entered. In every iteration of this loop is a single timestep that has four basic elements. First, it prepares to take a timestep by remeshing the model if necessary. Second, it adjusts the model to reflect mass loss by winds or mass gain from accretion. This step also adjusts abundances for element diffusion, determines the convective diffusion coefficients and solves for the new structure and composition using a solver. Thirdly, the next timestep is estimated. Lastly in the fourth part the output files are generated. Further details of this process can be found in the Instrument paper Paxton et al. (2011).

MESA includes some saved models for convenience. In this project a pre-main sequence model is generated for the initial case. This creates a model with uniform composition with the given mass, a core temperature below $10^6 K$ so no nuclear burning, and uniform contraction for enough luminosity to make it fully convective. Other initial parameters such as initial hydrogen fraction, He fractions, metallicity, etc. are taken from the inlist which is different for each model that is run.

In the Solar calibration case the model is run till the known age of the Sun is reached. Then a χ^2 (χ^2 is not to be confused with the χ used for thermometric conductivity defined below) is calculated by comparing known observables in the Sun and which is used to search for a good solar model. This is done using a modified version of MESA's `simplex_solar_calibration` example provided in their test suite.

A major part of this thesis involves running many MESA models for different stars and different parameters. This process was partially automated by using a python script to create the inlists for subsequent runs. In this case the termination condition for the model is when the $\Delta\nu$ of the model reaches the observed $\Delta\nu$ of the star that is being studied it is stopped. It was later found that if the timestep was too large the model stops at a very different $\Delta\nu$. However, lowering the timestep for the whole run would increase the runtime of the simulation too much. To save time a modification was made using the `run_star_extras.f90` file that lowered the timestep when near the models were near the expected $\Delta\nu$. These models were run using both Canuto-Mazzitelli's and Canuto-Goldman-Mazzitelli's models of turbulent convection (detailed in Section 3.2.1).

Most parts of the MESA simulation include hooks that allow the user to change the way MESA handles the simulation. For example, the user can configure when and how frequently data are outputted to disk if the model produces too much or too little data. In this thesis this feature was to be used to implement two extra models of convective turbulence. However, due to a bug in the MESA source code in the latest version at the time, this was not possible. I implemented these two models, as part of this project, directly into the MESA source code.

3.2 Treatment of Convective Turbulence

3.2.1 Canuto-Mazzitelli Model

Comparison of theories of stellar evolution and observational data became feasible after Biermann (1948), Vitense (1953) and others proposed the adoption of the mixing-length theory (henceforth MLT) to treat the turbulent convection in stars. Convective turbulence in the interior of stars is characterised by eddies of all sizes. MLT makes the assumption that there is only one large eddy. Despite this simplification, along with its single adjustable parameter, MLT has managed to do a good job in simulating stellar interiors and has found considerable use in this field. This is partly due to the fact that in most of the stellar interior the gradient is quite close to adiabatic which can be well modelled by varying the free parameter to match the radius and luminosity.

While MLT has been useful, it is still an incomplete approximation. Even if an exact solution is still difficult a better approximation is definitely possible as shown by Canuto and Mazzitelli (1991). The Canuto-Mazzitelli Model (henceforth referred to as the CM Model) seeks to solve two problems with the MLT. The first being the principal assumption of MLT which is that there is only a single large eddy in the fluid. It can be shown that this approximation is reasonable satisfied in extremely viscous fluids. However, the interior of stars are nearly inviscid which makes the MLT a poor fit for modelling them. The second problem is with the arbitrary nature of the adjustable parameter mixing length Λ. The MLT does not provide any justification or method of obtaining Λ other than varying it to match known values. It is also shown that under incompressible conditions and high convective efficiency the equations do not provide a natural unit of length which can be used to set the mixing length.

The CM model solves the first problem by deriving the full spectrum of turbulent eddies as an arbitrary closure of moments, which is used to calculate a new expression for convective flux. The second problem is solved by proposing a value for the mixing length $\Lambda = \alpha \cdot H_p$ where, H_p is the pressure scale height and α is an adjustable parameter that is calibrated using a solar model. While this adjustable parameter undermines the point of trying to eliminate an arbitrary parameter, this method makes this parameter smaller than 1 in the Sun and adds more physical meaning to the mixing length where the eddies are smallest near the top and get larger with depth. A more physically reasoned way of handling this could be to set $\Lambda = z$ where z is the distance from any point in the convective zone to the top of it. This is shown to fit the Sun to within 0.2% which MLT fails to do for a similar mixing length. Another advantage of this method is that it is falsifiable. If this expression for mixing length fails to model a star, then the physics it is built on do not apply to that star. This is a problem with MLT as a good model does not tell you anything about the physics of the star.

Another advantage of the CM model is that the changes between MLT and the new model are quite simple, with the biggest being a change to the equation to solve to obtain the convective efficiency Γ. This allows a simple implementation to existing code that implements MLT. In MLT this equation is a simple cubic equation,

$$a_0\Gamma^3 + \Gamma^2 + \Gamma - \delta = 0, \tag{3.1}$$

here $a_0 = 9/4$ and Γ is a variable defined by Σ as given in Equation (3.5) which is in turn related to the superadiabatic gradient as follows

$$\Sigma = 4A^2 \left(\nabla - \nabla_{ad}\right). \tag{3.2}$$

In the CM model we replace this equation with

$$a_0\Omega\left(\Gamma\right)\Gamma^3 + \Gamma^2 + \Gamma - \delta = 0, \tag{3.3}$$

where

$$\Omega\left(\Sigma\right) = \frac{\phi}{\phi^{\mathrm{MLT}}}, \tag{3.4}$$

$$\Sigma = 4\Gamma\left(\Gamma + 1\right), \tag{3.5}$$

$$\phi^{\mathrm{MLT}} = \frac{1}{2}a_0\Sigma^{-1}\left[\left(1+\Sigma\right)^{1/2} - 1\right]^3, \tag{3.6}$$

$$\phi = a_1\Sigma^m\left[\left(1 + a_2\Sigma\right)^n - 1\right]^p, \tag{3.7}$$

$$\delta = A^2 \left(\nabla_r - \nabla_{ad}\right), \tag{3.8}$$

$$A = \frac{\Lambda^2}{9\chi}\left(\frac{g}{2H_p}\right)^{1/2}, \tag{3.9}$$

$$a_1 = 24.868, \quad a_2 = 9.7666 \times 10^{-2},$$
$$m = 0.14972, \quad n = 0.18931, \quad p = 1.8503,$$

where Λ is the mixing length, $\chi = K/c_p\rho$ is the thermometric conductivity, g is gravitational acceleration and H_p is the pressure scale height. In this model Λ can be taken as αH_p or z where z is the distance to the top of the convective layer. For this thesis the mixing length is taken as $\Lambda = \alpha \cdot H_p$ to give us another free parameter to tune through modelling.

The CM model also provides different expressions for convective velocity and turbulent pressure. Equation (41) of Canuto and Mazzitelli (1991) gives the convective velocity as

$$v_t = \left(\frac{\chi}{\Lambda}\right)\sqrt{2S}, \tag{3.10}$$

where S is given by Equation (7) of Canuto and Mazzitelli (1991) as

$$S = (81/2)\,\Sigma. \tag{3.11}$$

The CM model also provides an expression for turbulent pressure however this wasn't implemented as it caused issues in the pre main sequence model creation. The continuation of this project is expected to deal with this issue. However, this is not expected to make a major difference to the model.

3.2.2 Canuto-Goldman-Mazzitelli Model

The Canuto-Goldman-Mazzitelli Model (henceforth CGM model), is a subsequent model of convective turbulence that seeks to formulate a self consistent model. The rate of energy input in the CM model was a source of improvement as the turbulence is expected to regulate the energy input from the source (buoyancy). The CM model does not account for this. This lack of feedback prevents the CM model from being self-consistent. However, since a self consistent model is a very complex problem implementing it comes with the trade-of of being forced to use simplified versions of the non linear interactions between eddies.

The model that results from these modifications is the CGM model. Following the derivations given in Canuto et al. (1996), we see that we can use the same Equation (3.3) with a different form for $\Omega\,(\Sigma)$ as

$$\Omega_{\rm CGM} = \frac{\Phi_{\rm CGM}}{\Phi_{\rm MLT}}, \tag{3.12}$$

where $\Phi_{\rm CGM}$ is defined below in Equation (3.19). Similar to CM model the CGM model specifies a different expression for convective velocity. The expression given is

$$v_t = \left(\frac{\chi}{\Lambda}\right)\sqrt{F_3(S)F_4(S)}, \tag{3.13}$$

where

$$F_3(S) = \left(\frac{K_0}{1.5}\right)^3 \frac{0.00101392 \cdot S^2}{1 + \sqrt{1 + 0.000017848 \cdot S^2}}, \tag{3.14}$$

$$F_4(S) = 6.39899 + \frac{2.256815\left(-1 + 0.000777055 \cdot S^{0.868589}\right)}{1 + 0.000777055 \cdot S^{0.868589}}. \tag{3.15}$$

3.2.3 Implementation

This model is not part of MESA's provided convection options. This necessitated implementing it ourselves. MESA provides a few ways to do this. One way of doing it is implementing a hook that will add a new MLT method by creating a `run_stars_extras.f90` file. This method was unfortunately not viable in this instance as the latest version of MESA at the time (r24.08.1) had a bug that made writing custom convection

implementations difficult [1]. As waiting for a fix would take too long, this project uses a modified version of the MESA source code that implements CM model. The code for the same is based on an old implementation [2] from the MESA mailing list by Dr. Warrick Ball. However, MESA has undergone many improvements since this mail was written. Much of the code had to be rewritten for the newer code. We majorly modify the file `$MESA_DIR/turb/private/mlt.f90` and the contained subroutine `calc_MLT`.

Since the CM and CGM model share the same a_0, convective and radiative conductivity and a dimensionless parameter A (ratio of convective and radiative conductivity) with the standard MLT prescription given by Cox and Giuli (1968), the calculation of these are left unchanged. As shown above the implementation of CM and CGM models differ from MLT mainly in the equation that is solved to obtain the convective efficiency Γ. In the case of MLT it is the cubic equation given by Equation (3.1). This needs to be replaced with the non-linear equation for the same provided by the CM and CGM models. Both CM and CGM have a similar form with the only difference being the definition of Ω

$$a_0 \Omega(\Gamma) \Gamma^3 + \Gamma^2 + \Gamma - \delta = 0. \tag{3.16}$$

The definition of Ω is also similar for both models with the only difference being the numerator

$$\Omega_{\rm CM} = \frac{\Phi_{\rm CM}}{\Phi_{\rm MLT}}, \qquad \Omega_{\rm CGM} = \frac{\Phi_{\rm CGM}}{\Phi_{\rm MLT}}. \tag{3.17}$$

The two numerators are

$$\phi_{\rm CM} = a_1 \Sigma^m \left[(1 + a_2 \Sigma)^n - 1\right]^p, \tag{3.18}$$

where

$$a_1 = 24.868, \quad a_2 = 9.7666 \times 10^{-2},$$
$$m = 0.14972, \quad n = 0.18931, \quad p = 1.8503,$$

and

$$\phi_{\rm CGM} = F_1(\Sigma) \cdot F_2(\Sigma), \tag{3.19}$$

$$F_1(\Sigma) = \left(\frac{K_0}{1.5}\right)^3 a \Sigma^k \left[(1 + b\Sigma)^m - 1\right]^n, \tag{3.20}$$

where K_0 is the Kolmogorov constant which we set to 1.5 and

$$a = 10.8654, \quad b = 0.00489073, \quad k = 0.149888,$$
$$m = 0.189238, \quad n = 0.185011,$$

and

$$F_2(\Sigma) = 1 + \frac{c\Sigma^p}{1 + d\Sigma^q} + \frac{e\Sigma^r}{1 + f\Sigma^t}, \tag{3.21}$$

where

$$c = 1.080\,71 \times 10^{-2}, \quad d = 3.012\,08 \times 10^{-3}, \quad e = 3.344\,41 \times 10^{-4},$$
$$f = 1.25 \times 10^{-4}, \quad p = 0.72, \quad q = 0.92, \quad r = 1.2, \quad t = 1.5.$$

We then use these functions in place of the MLT equation (Equation (3.1)) in the source code. Since unlike the MLT equation these functions are non linear they need to be solved using root finding methods. MESA provides utilities for doing the same and the routine `safe_root_with_initial_guess` is used from the `num` module. The routine also requires the first order derivatives of Γ, this is calculated analytically based on which model is

[1] This bug was reported to the MESA github (https://github.com/MESAHub/mesa/issues/874). At the time of writing the fix for the same as has been approved and will be included in the next release version.

[2] The email is archived here: https://sourceforge.net/p/mesa/mailman/message/33552129/.

selected. We then use the same formulas for calculating average convective velocity and diffusion coefficient D as the Cox and Giuli implementation.

$$\bar{v} = \alpha \sqrt{\frac{Q * P}{8 * \rho}} * \frac{\Gamma}{A}, \tag{3.22}$$

$$D = \bar{v} \cdot \frac{\Lambda}{3}, \tag{3.23}$$

where

$$Q = -\left[\left(\frac{\partial \ln \rho}{\partial \ln \mu}\right)_{\mathrm{P,\ T}} \left(\frac{\partial \ln \mu}{\partial \ln \mathrm{T}}\right)_{\mathrm{P}} + \left(\frac{\partial \ln \rho}{\partial \ln \mathrm{T}}\right)_{\mu,\mathrm{T}}\right]. \tag{3.24}$$

It is to be noted that the CM and CGM models do provide a different expression for convective velocity as mentioned previously. However, since they weren't expected to create a significant difference in the models they were omitted for this part of the project. While the implementation of convective velocity might have been straightforward, the turbulent pressure had its own complications. The pre main sequence model generation, which was the first step in all the modelling performed for this project, would fail for any non zero turbulent pressure factor greater than ≈ 0.1 [3]. The CM model without convective velocity and turbulent pressure was tested by Dr. Warrick Ball in his initial implementation, so to maintain consistency both convective velocity and turbulent pressure were left the same as MLT. The implementation of these features will be incrementally tested in the future as part of continuation of this work.

We now calculate the value for the quantity ζ given by Equation (14.78) in Cox and Giuli (1968) as

$$\zeta = \frac{\nabla_r - \nabla}{\nabla_r - \nabla_{ad}}. \tag{3.25}$$

For MLT the expression for ζ can be found in Equation (14.80) of Cox and Giuli (1968) as

$$\zeta = \left(\frac{\Gamma}{B}\right)^3, \tag{3.26}$$

where

$$B = \left[\left(A^2/a_0\right)\left(\nabla_r - \nabla_{ad}\right)\right]^{1/3}. \tag{3.27}$$

For both CM and CGM we use the expression

$$\zeta = \frac{\phi_{\mathrm{CM}}}{1 + \phi_{\mathrm{CM}}}. \tag{3.28}$$

This value is then used to calculate the temperature gradient as follows

$$\nabla T = (1 - \zeta)\,\nabla_r + \zeta \nabla_L, \tag{3.29}$$

where ∇T is the temperature gradient $\frac{\partial \ln T}{\partial \ln P}$, ∇_r is the radiative temperature gradient $\frac{\partial \ln T}{\partial \ln P}$, which is value of temperature gradient required to transmit the entire flux by radiation and ∇_L is Ledoux temperature gradient $\frac{\partial \ln T}{\partial \ln P}$.

All these modifications have been uploaded to a fork of the official MESA repository at `https://github.com/VishalVSV/mesa`. This fork is a clone of the release `r24.08.1` with the CM and CGM model implemented. In the future the convective velocity and other features will be updated to this repository. Anyone can clone the repository and use it as an in place replacement for their installation of MESA. The code will have to be compiled with the MESA SDK version `24.7.1`[4].

[3] From discussions with the MESA user list it was suggested that the turbulent pressure be omitted for the pre main sequence steps. However, this could not be implemented in time for this project.

[4] This can be found at `http://user.astro.wisc.edu/~townsend/static.php?ref=mesasdk`

3.2.4 Calibration

The implementation of the CM model used in this work includes an adjustable parameter α. A calibrated value for this parameter should be determined as a test of this implementation. MESA is used to calibrate α by attempting to find a good solar model using the implemented CM model. This is done by modifying the test suite example `simplex_solar_calibration` that is included with MESA. The parameter `MLT_option` in the inlist is set to `"CM1991"` and later `"CGM1996"`. The initial FeH, which is a measure of the initial metallicity, was also varied. These values are varied using a simplex search algorithm till the χ^2 difference between the observables and model values (log luminosity and log radius) is sufficiently small. This process will settle on an α for which the solar model matches well. Whether this value will generalize to non main sequence stars is debatable, as in this thesis it was found that models with good agreement to the observed data were found with α nearly double the calibrated α value.

The resulting simplex search settles on the value $\alpha = 0.984$ for the CGM model, which is interestingly different from the value $\alpha = 0.64$ proposed by Deheuvels et al. (2012). This could be due to the convective velocity which was left on the MLT expressions. This will be tested in the continuation to this project.

4. GYRE

GYRE is a stellar oscillation code that calculates the eigenfunctions and eigenfrequencies for the normal modes of a given model (Townsend and Teitler, 2013). These data are used to compare with observed frequencies of the star in question. This allows constraints on the physical parameters of the star that are difficult to observe directly such as radius, mass, age, etc. GYRE accepts input in many formats but we will use the output of MESA directly as an input of GYRE.

GYRE uses a method called 'Magnus Multiple Shooting' (MMS) to solve the required boundary value problem defined by a system of linear, homogeneous, first-order differential equations. The method is described in more detail in Section 3 of Townsend and Teitler (2013).

We run GYRE on the last 12 models of an evolutionary model to save on time and disk space. Using a Fortran namelist we pass the settings over to GYRE. We set it to scan 200 points linearly in inverse frequency space from $\nu_{max} - 4 \cdot \Delta\nu$ to $\nu_{max} + 4 \cdot \Delta\nu$. ν_{max} is a "highest frequency" that is determined by a scaling relation using the Sun's highest observed frequency

$$\nu_{max} = \nu_{\odot max} \cdot \frac{M}{\mathrm{M}_\odot} \cdot \left(\left(\frac{R}{\mathrm{R}_\odot} \right)^2 \left(\frac{\mathrm{T_{eff}}}{\mathrm{T}_{\odot eff}} \right)^{0.5} \right)^{-0.5} . \tag{4.1}$$

We also set it to only search for $l = 0, 1, 2$ modes as they are the only modes that we can obtain observational data for. We also set the outer bound condition to vacuum which is what is required to use $\delta p = 0$ as the boundary condition.

5. Surface Correction

5.1 Introduction

While the CM model does improve the accuracy of the computed models by a significant amount, the fact remains that it is still an approximation of what actual turbulent convection would behave like. This discrepancy shows up as a systematic difference between observed frequencies and model frequencies. This can be easily seen in the case of the Sun as with the abundant information available one can efficiently separate this systematic discrepancy.

Surface correction methods deal with this systematic discrepancy by fitting the difference between the observed frequencies and their closest counterparts in the computed model. This process requires a model that is already close to the observed values. This difference is expected to follow a good trend if it is mainly due to surface corrections.

This difference between the model and observed frequencies is usually modelled in two different ways. One is the power law method proposed by Kjeldsen et al. (2008) or the newer method proposed by Ball and Gizon (2014). Both methods work in similar ways but differ in the function used to fit the difference.

In the power law method the function used to fit the difference is

$$\nu_{obs}\left(n\right) - \nu_{model}\left(n\right) = \left(a\left[\frac{\nu_{obs}\left(n\right)}{\nu_0}\right]^b\right) / \, I, \tag{5.1}$$

where ν_0 is a suitably chosen reference parameter and a and b are parameters to be determined. The newer method propsed by Ball and Gizon (2014) uses a different function,

$$\nu_{obs}\left(n\right) - \nu_{model}\left(n\right) = \left(a_{-1}\left[\frac{\nu_{obs}\left(n\right)}{\nu_0}\right]^{-1} + a_3\left[\frac{\nu_{obs}\left(n\right)}{\nu_0}\right]^3\right) / \, I, \tag{5.2}$$

where a_{-1} and a_3 are the parameters to be determined. In both models I is the normalized mode inertia that is defined by Aerts et al. (2010) Eq. (3.140) which is

$$I = 4\pi\frac{\int_0^R \left[\left|\xi_r(r)\right|^2 + l(l+1)\left|\xi_h(r)\right|^2\right]\rho r^2\, dr}{M\left[\left|\xi_r(r)\right|^2 + l(l+1)\left|\xi_h(r)\right|^2\right]}. \tag{5.3}$$

From the GYRE output we use the equation

$$I = \frac{E_p + E_g}{E_p}, \tag{5.4}$$

to the same effect. This value is near 1 for p-mode frequencies and above 1 for the mixed modes[1]. Since all the frequencies we observe in the Sun are p modes this mode inertia will be unity and can be ignored but in Red Giants with observed mixed modes this value becomes important.

[1] It is to be noted that the symbols used for this mode inertia vary and it is also called Q_{nl} in some literature such as Christensen-Dalsgaard.

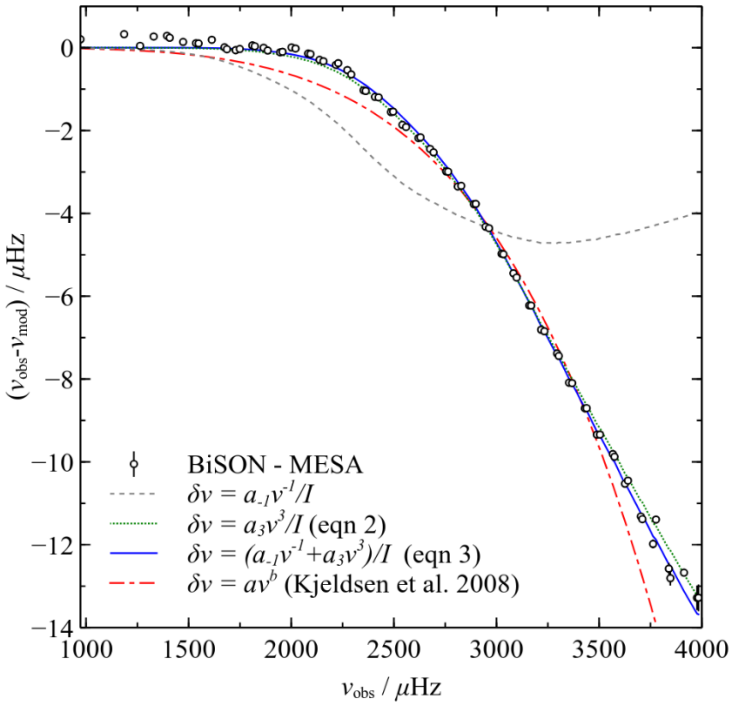

Figure 5.1: This plot shows the performance of various methods of fitting the difference in frequencies. We see that the inverse term on its own does not fit the difference well but with the cubic term becomes a better fit at higher frequencies.
Figure taken from Ball and Gizon (2014) (Fig 2).

5.2 Application to Red Giants

Application of surface corrections to red giants isn't as straightforward as it is for the solar case as unlike the Sun they contain mixed modes. This makes the normalized mode inertia I in the correction non trivial and consequently very important. A selection of model frequencies is provided in Table (5.1). It is noted that in these frequencies the correction is most significant for the $l = 0$ modes. This is due to the fact that all the corrections are weighted by the factor I (Equation 5.3). This factor is nearly unity for $l = 0$ modes. Which allows the corrections to be applied fully. For mixed modes and g modes this value is larger than 1 and in the case of g modes it is much larger than 1. We can see this in effect as the $l = 2$ g dominated modes have hardly any correction. This can be seen from the definition of the normalized mode inertia as the denominator is small for g modes.

Degree (l)	Mode Frequencies (μHz)	Corrected Frequencies (μHz)	Observed Frequencies (μHz)
0	252.421	238.773	
0	278.871	268.616	
0	305.881	298.012	
0	333.327	327.17	327.17
0	360.849	355.939	355.929
0	388.677	384.703	384.432
0	416.806	413.545	413.322
0	445.076	442.368	442.576
1	232.528	229.783	
1	237.408	232.138	
1	241.87	237.786	
1	247.5	245.651	
1	253.976	252.438	
1	260.477	257.594	
1	265.741	260.975	
1	271.451	269.266	
1	278.956	277.655	
1	286.712	284.317	
1	292.68	288.693	
2	229.61	229.454	
2	233.189	233.083	
2	236.886	236.781	
2	240.696	240.543	
2	244.597	244.158	
2	248.086	241.3	
2	249.432	243.605	
2	253.147	252.789	
2	257.467	257.343	
2	261.973	261.88	
2	266.637	266.511	

Table 5.1: Some selected model frequencies for a model calibrated to KIC 7341231.
These frequencies are generated using the MESA model output as input to GYRE. . A power law correction was applied to the frequencies. The good performance of this fit is expected though since 5 frequencies are fitted to just 2 parameters. A good fit is expected numerically. A better test would be to include all the observed frequencies but this is complicated as it is not sure what the treatment of mixed modes should be in the fitting process.

6. Results

6.1 Solar Model

To calibrate the parameter α for the CM model a simplex search was performed using MESA's tools which searched for a model that would closely match the observed solar values, while varying the α and initial metallicity. A relatively lower value of α is expected when compared to MLT as the CM model has larger flux and can more efficiently account for the convection at a lower α. We find the best fit by calculating a χ^2 for every model that compares the luminosity $\log(L)$ and radius $\log(R)$ (both values are in solar units which means they need to be as close to 0 as possible for a best fit). In the calibration that was performed, the final model had a log radius of -2.776×10^{-5} which is about $0.9999\,\mathrm{R}_\odot$ and a log luminosity of 1.395×10^{-3} which is about $1.003\,\mathrm{L}_\odot$. This led to a final χ^2 of around 0.5.

The best fit had the following parameters.

α	0.98478
`init_FeH`	0.05888
`init_Y`	0.26955
$\mathrm{T_{eff}}$	5776

Here α is the CM mixing length parameter which is multiplied with the pressure scale height to get the mixing length, `init_FeH` is a measure of initial surface metallicity defined by

$$[\mathrm{Fe/H}] = \log_{10}\left(\frac{Z}{X} \cdot \frac{X_\odot}{Z_\odot}\right). \tag{6.1}$$

It is to be noted that the solar fraction in this expression is a semi arbitrary value and the final value need not be near 0 to show a convergence to a solar model. `init_Y` is the initial He fraction in the model. $\mathrm{T_{eff}}$ is the effective surface temperature.

This is not directly useful for the stellar modelling done in this project as there is no reason Red Giants will have similar mixing length factors, but it gives us a good starting point to verify if the model is functioning well. The calibrated α, while larger than suggested in Canuto and Mazzitelli (1991), is still much lower than the MLT case which is what is important.

6.2 KIC 7341231

For the modelling of KIC 7341231 we define a χ^2 expression which will allow us to compare observables and select a best fit model. To this end we compare effective temperature $\mathrm{T_{eff}}$, large frequency separation $\Delta\nu$, period separation $\Delta\Pi$ and surface gravity $\log(g)$. This yields the expression

$$\chi^2 = \frac{(\mathrm{T_{eff,\,obs}} - \mathrm{T_{eff}})^2}{\sigma^2(\mathrm{T_{eff}})} + \frac{(\Delta\nu_{\mathrm{obs}} - \Delta\nu)^2}{\sigma^2(\Delta\nu)} + \frac{(\Delta\Pi_{\mathrm{obs}} - \Delta\Pi)^2}{\sigma^2(\Delta\Pi)} + \frac{(\log(g)_{\mathrm{obs}} - \log(g))^2}{\sigma^2(\log(g))}. \tag{6.2}$$

From Deheuvels et al. (2012) we get the observed values as follows

$$\mathrm{T_{eff}} = 5470 \pm 150\ \mathrm{K}, \qquad \log(g) = 3.55 \pm 0.03,$$
$$\Delta\nu = 28.9 \pm 0.2\ \mu\mathrm{Hz}, \qquad \Delta\Pi = 107.1 \pm 2.3\ s.$$

Finding the model that minimizes this χ^2 gives us the following model

Mass ($M_\odot$)	0.880
Inital Z	0.00239
Inital Y	0.2527
T_{eff} (K)	5567
log g	3.523
$\Delta\nu$ (μHz)	28.907
$\Delta\Pi$ (s)	108.316
Radius ($R_\odot$)	2.68
Stellar Age (Gyr)	9.8
Convection Model Used	CGM
α_{CGM}	1.2
χ^2	1.27

Table 6.1: Best fit Model for KIC 7341231 found through MESA modelling

We notice that the α is higher than 1. This is assumed to be due to the fact that the convective flux could be much higher in Red Giants when compared to the Sun. It is also noted that the stellar age is well constrained by the mass of the star as the age did not significantly vary when other parameters were changed. This is expected for Red Giants. Yet the stellar age does not match the values given in Deheuvels et al. (2012) for the same mass. In Deheuvels et al. (2012) the reported value for the model with $0.880\,M_\odot$ (Model A in their paper) is 11.3 Gyr. This difference is something that has not yet been fully understood. The source of this difference is of great importance as the difference in age is significant and if this is due to computational differences in modelling techniques it must be well understood to properly study this method of constraining stellar age.

It is also interesting to note that the CGM model appears to yield better models across nearly all the implementations. This does yield some confidence in the fact that the self consistent interpretation makes a valid improvement in the modelling.

7. Further Work

7.1 A complete implementation of CM and CGM models

The CM and CGM models used in this thesis were partially incomplete. While they were enough to yield an improvement over MLT, there is definitely room for improvement. Notably, the convective velocity and turbulent pressure have been given alternate expressions in the CM and CGM models. This was not implemented for this project. Another major feature that wasn't implemented was setting mixing length to the distance to the top of the convective layer. It is possible that this non-local theory could yield significant differences in red giants where the convective layer is much larger than solar case. These improvements will be included in the continuation of this project.

7.2 Reinforcement Learning Based Modelling

The grid modelling approach to stellar modelling may work well for a single star but is too slow and resource intensive to scale to analysis of many stars. A possible way of solving this problem is to use reinforcement learning to guide the parameters in the process of modelling. It is expected that this will yield similar results but without the extra computation and excess time that grid modelling would entail.

7.3 Improved Spectrum Fitting

The current method of fitting the spectrum observed has certain gaps in understanding. Allowing ϵ_g, a phase factor in spectrum analysis that has not been discussed in this thesis, to vary allows for an extremely good fit. This is discussed in a recent paper Liagre et al. (2025), where they allow ϵ_g to vary and find $\epsilon_{g,1}$ for $l = 1$ modes and $\epsilon_{g,2}$ for $l = 2$ modes can vary by over 50%. There is an ongoing discussion with the group who wrote this paper and other scientists regarding whether this is physically reasonable, as we would intuitively expect this parameter to not vary significantly between the two degrees. These spectra are difficult to parse due to various reason such as near-degeneracy which occurs when the large frequency separation is off the order of rotation rate. This new method of improving the spectrum fitting hasn't been taken into account here as the results only came out near the end of the thesis work.

8. Bibliography

Conny Aerts, Jørgen Christensen-Dalsgaard, and Donald W. Kurtz. *Asteroseismology*. 2010. doi: 10.1007/978-1-4020-5803-5.

W. H. Ball and L. Gizon. A new correction of stellar oscillation frequencies for near-surface effects. *A&A*, 568: A123, August 2014. doi: 10.1051/0004-6361/201424325.

Ludwig Biermann. Konvektion in rotierenden Sternen. *ZA*, 25:135, January 1948.

William J. Borucki, David Koch, Basri, et al. Kepler Planet-Detection Mission: Introduction and First Results. *Science*, 327(5968):977, February 2010. doi: 10.1126/science.1185402.

V. M. Canuto and I. Mazzitelli. Stellar Turbulent Convection: A New Model and Applications. *ApJ*, 370:295, March 1991. doi: 10.1086/169815.

V. M. Canuto, I. Goldman, and I. Mazzitelli. Stellar Turbulent Convection: A Self-consistent Model. *ApJ*, 473: 550, December 1996. doi: 10.1086/178166.

Jørgen Christensen-Dalsgaard. Lectures on stellar oscillations. https://users-phys.au.dk/~jcd/oscilnotes/Lecture_Notes_on_Stellar_Oscillations.pdf.

J. P. Cox and R. T. Giuli. *Principles of stellar structure*. 1968.

S. Deheuvels, R. A. García, W. J. Chaplin, S. Basu, Antia, et al. Seismic Evidence for a Rapidly Rotating Core in a Lower-giant-branch Star Observed with Kepler. *ApJ*, 756(1):19, September 2012. doi: 10.1088/0004-637X/756/1/19.

L. G. Henyey, L. Wilets, K. H. Böhm, R. Lelevier, and R. D. Levee. A Method for Automatic Computation of Stellar Evolution. *ApJ*, 129:628, May 1959. doi: 10.1086/146661.

Hans Kjeldsen, Timothy R. Bedding, and Jørgen Christensen-Dalsgaard. Correcting Stellar Oscillation Frequencies for Near-Surface Effects. *ApJL*, 683(2):L175, August 2008. doi: 10.1086/591667.

B. Liagre, A. Desai, L. Einramhof, and L. Bugnet. Near-degeneracy effects in quadrupolar mixed modes. from an asymptotic description to data fitting, 2025. URL https://arxiv.org/abs/2511.05314.

B. Paxton, L. Bildsten, A. Dotter, F. Herwig, P. Lesaffre, and F. Timmes. Modules for Experiments in Stellar Astrophysics (MESA). *ApJS*, 192:3, jan 2011. doi: 10.1088/0067-0049/192/1/3.

R. H. D. Townsend and S. A. Teitler. GYRE: an open-source stellar oscillation code based on a new Magnus Multiple Shooting scheme. *MNRAS*, 435(4):3406–3418, November 2013. doi: 10.1093/mnras/stt1533.

E. Vitense. Die Wasserstoffkonvektionszone der Sonne. Mit 11 Textabbildungen. *ZA*, 32:135, January 1953.